ELSEVIER

Chemical Engineering Science 62 (2007) 3008–3018

Chemical Engineering Science

www.elsevier.com/locate/ces

Effect of bubble size in turbulent bubbly downflow in a vertical channel

Jiacai Lu*, Gretar Tryggvason

Worcester Polytechnic Institute, Worcester, MA 01609, USA

Received 17 May 2006; received in revised form 30 December 2006; accepted 9 February 2007
Available online 25 February 2007

Abstract

The effect of bubble size on the properties of downward turbulent flows of bubbly liquids in a vertical channel is examined using direct numerical simulations, where the full Navier–Stokes equations are solved by a parallelized front-tracking/finite-volume method. The turbulent channel flow is driven downward by an imposed constant pressure gradient, and the friction Reynolds number, based on the friction velocity and half-width of the channel, is 127.3. Bubbles of two different sizes, with diameters of 31.8 and 38.2 wall units, are introduced into the turbulent flow with a monodisperse or bidisperse distribution. The results show that for the cases studied here the bubble size has little effect on the void fraction distribution and the mean vertical velocity profile. The average velocity fluctuations and the vorticity profiles across the channel do, however, change.

Keywords: Direct numerical simulations; Bubble size; Bubbly flow; Turbulent channel flow

1. Introduction

Turbulent bubbly flows in pipes or channels are found in a number of applications in the power, chemical, food, pharmaceutical and other industrials. Knowledge of the interaction between the bubbles and the turbulent flow is of great importance for the design and safety of these applications. In the past, many experimental studies have been carried out to study the void fraction distribution, average velocity profile, interfacial area, and the various properties of turbulent bubbly flows in vertical pipes or channels (Kashinsky and Randin, 1999; Liu and Bankoff, 1993 a,b; Nakoryakov et al., 1996; Oshinowo and Charles, 1974; Serizawa et al., 1975 a,b; Sun et al., 2004; Wang et al., 1987). These results indicated that the turbulence augmentation or reduction, after the introduction of the bubbles, depends on the void fraction and flow rates. However, some discrepancies have been found among these results, even under similar flow conditions. Serizawa et al. (1975 a,b) pointed out that different bubble size distributions resulted in different void fraction profiles: "wall-peaking", "coring" and "saddling". The experiments of Liu (1993) and Liu and Bankoff (1993 a,b) showed that identical flow condition but different bubble sizes resulted in different local hydraulic characteristics such as void fraction distribution and turbulent structure. Nakoryakov et al. (1996) studied the effect of bubble size on flow parameters both in upflow and downflow. Liu (1997) studied the effect of bubble size on the behavior of the turbulent shear stress close to the wall. Felton and Loth (2002) investigated the motion of bubbles of different sizes in a vertical turbulent boundary layer. They observed sliding, bouncing or freely dispersing bubbles in the boundary layer and measured the different void fraction distributions. A further exploration of the effect of bubble size was conducted by Tomiyama et al. (2002). They used a large range of bubble diameters to study the transverse migration of bubbles in an upward shear flow. It has been clarified through a number of experiments that the lateral migration of bubbles strongly depends on bubble size, i.e., in upward pipe or channel flows, small bubbles tend to migrate toward the pipe wall and cause a wall-peaked bubble distribution, whereas large bubbles tend to migrate toward the pipe center, resulting in a core-peaked bubble distribution. However, most of the previous investigations considered the case of upward bubbly flow, and only a few investigations have been performed for downward flows. Wang et al. (1987) and Kashinsky and Randin (1999) showed results for the void fraction distribution, liquid velocity

* Corresponding author. Tel.: +1 508 8316405; fax: +1 508 8315680.
E-mail address: jlu@wpi.edu (J. Lu).

0009-2509/$ - see front matter © 2007 Elsevier Ltd. All rights reserved.
doi:10.1016/j.ces.2007.02.012

profile and turbulent structures of downward turbulent bubbly flows, but information about the effect of bubble size on downward turbulent bubbly flows is still limited.

Many analytical studies have also been carried out to predict the structure of bubbly flows. Bankoff (1960) was one of the first to analyze the lateral void fraction distribution for a bubbly flow by assuming a power law distribution for both the velocity and the void fraction based on a variable-density single-fluid model. Levy (1963) introduced a model based on Prandtl's mixing-length theory to predict the density distribution of a turbulent bubbly flow. Later, many predictions have been done using a drift-flux model (Clark and Flemmer, 1985) and two-fluid models (Drew and Lahey, 1979, 1982; Lopez de Bertodano et al., 1994) for bubbly flows, with a high degree of success. In general, these models only include one bubble size, which is specified as an input parameter, and the bubble size distribution can therefore not be predicted. Although models of turbulent polydisperse bubbly flow in vertical channels have been used to predict the change of the void fraction profile that takes place as the bubble size increases (Politano et al., 2003), these models are still very limited.

Direct numerical simulation (DNS), where the flow field is found by solving the governing equations numerically on sufficiently fine grids so that all details (including the shape of the bubbles and the flow around them) are fully solved, is an useful tool to improve the current understanding of the local and instantaneous properties of bubbles and turbulence. DNS of homogeneous buoyancy-driven bubbly flows with nearly spherical and deformable bubbles have been done by Tryggvason and co-worker (Bunner and Tryggvason, 2002 a,b, 2003; Esmaeeli and Tryggvason, 1998, 1999, 2005). In our previous studies, we already used DNS to examine laminar bubbly flows in vertical channels (Lu et al., 2006) and found that the lateral migration of nearly spherical bubbles resulted in two regions: a core region with a nearly constant average liquid velocity and void fraction and a wall layer that is bubble-free for downflow and bubble-rich for upflow. The void fraction in the core region is always such that the weight of the liquid/bubble mixture is balanced by the imposed pressure gradient, and the velocity fluctuations and the rise velocity of bubbles matched the results for the corresponding homogeneous flow. We also examined the effect of the average void fraction on a downward turbulent bubbly flow using DNS (Lu and Tryggvason, 2006). The results showed that most of the characteristics of laminar bubbly downflows carried over to turbulent downflows, although the turbulent structures are different. One difference is that the boundaries between the core and the wall layer for turbulent bubbly downflows are not as sharp as for laminar downflows. In that paper, the bubble sizes are the same for all cases.

In this paper, we use different size bubbles, but the same average void fraction, to gain further knowledge of the effect of bubble size on the void fraction profile, the liquid velocity distribution and the turbulence modification in downward turbulent bubbly flows. We perform DNS of downward turbulent flows with monodispersed or bidispersed bubbles in a vertical channel using two bubble sizes. The smaller bubbles are nearly spherical, whereas the bigger ones are slightly ellipsoidal.

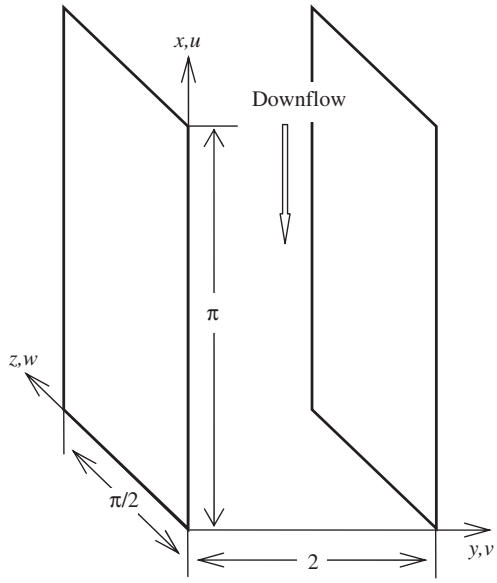

Fig. 1. A sketch of the flow configuration studied here.

2. Problem specification and numerical method

We consider a turbulent flow in a vertical channel, shown schematically in Fig. 1. The channel is bounded by two parallel vertical walls and we align a coordinate system such that x is in the streamwise direction, y in the wall-normal direction and z the spanwise direction. The direction of the streamwise velocity is also shown in the figure. The channel width is $H=2\delta=2$, the length of the computational domain in the streamwise direction is π and $\pi/2$ in the spanwise direction. The flow is assumed to be periodic in both the streamwise and the spanwise direction, and no-slip boundary conditions are applied to the walls.

The flow is driven downward by an imposed constant pressure gradient $\mathrm{d}p/\mathrm{d}x$, and gravity g acts in the negative streamwise direction. At steady state, the average wall shear stress τ_w is related to the pressure gradient and the weight of the bubble/liquid mixture via a streamwise momentum balance according to

$$\tau_w = (\mathrm{d}p/\mathrm{d}x + \rho_0 g)\delta = \beta\delta. \tag{1}$$

Here, δ is the half-width of the channel, ρ_0 is the average density of the mixture, and $\beta = \mathrm{d}p/\mathrm{d}x + \rho_0 g$ is the sum of the pressure gradient and the volumetric weight of the mixture. Since the liquid and the bubbles are taken to be incompressible, ρ_0 is constant. The value of β is therefore constant due to the constant pressure gradient $\mathrm{d}p/\mathrm{d}x$ imposed on the bubbly flow. The direction of the flow depends directly on the sign of β. In all simulations reported in this paper, β is taken to be 0.0018, resulting in a downward flow. Since the half-width of the channel δ is 1, we therefore get the average wall shear stress $\tau_w = 0.0018$. This value will be used to check whether the turbulent bubbly flow is at statistically steady state.

Table 1
Parameters comparison for the liquid–bubble system used in the simulations and the water–air bubbles system

Parameters	Liquid–bubble system used in the simulations	Water–air bubble system (20 °C)
Channel size (x, y, z)	π, 2, $\pi/2$	19.22 mm, 12.24 mm, 9.61 mm
Bubble size	0.25/0.30	1.53 mm/1.84 mm
Average velocity	0.63	0.31 m/s
Morton number	1.54×10^{-10}	2.52×10^{-11}
Eötvös number	0.31/0.45	0.31/0.45
Channel Reynolds number	3786	3786

The liquid density is $\rho_l = 1$ and the liquid kinematic viscosity is $\nu_l = 1/3000$. The friction velocity is therefore $u^+ = \sqrt{\tau_w/\rho_l} = 0.0424$, and the friction Reynolds number, based on the friction velocity and the half-width of the channel, is $Re^+ = u^+\delta/\nu_l = 127.3$. The channel Reynolds number, based on the average velocity ($U = 0.63$) of a flow without bubbles and the width of the channel, is $Re = UH/\nu_l = 3786$. In terms of wall units, defined by $l_0^+ = \nu_l/u^+$, the size of the channel is $400 \times 254.6 \times 200$ in the x-, y- and z-direction, respectively. This is a so-called "minimum turbulent channel", and represents the smallest channel that can sustain turbulence (Jimenez and Moin, 1991). The advantage of using this "minimum turbulent channel" is that it allows us to perform simulations of a turbulent flow with a minimal amount of computational effort. To make the simulations as easy as possible, the density of the bubbles is taken to be one-tenth of the liquid density. The dynamic viscosity of the bubbles and of the liquid are taken to be equal, so the kinematic viscosity of the bubbles is 10 times that of the liquid, comparable to what it is for air and water. The surface tension is $\sigma = 0.02$ and the gravity acceleration is $g = 0.1$. The Morton number, $M = g\mu_l^4/\rho_l\sigma^3$, is therefore 1.54×10^{-10}. The Morton number is slightly higher than for an air bubble in water ($M = 2.52 \times 10^{-11}$ at 20 °C), but could be matched by using an aqueous solution of sugar in water (Stewart, 1995). Two sizes of bubbles are simulated in this paper. The diameter of the small bubbles is $d_0 = 0.25$ or 31.8 wall units, and the big bubbles' diameter is $d_0 = 0.3$ or 38.2 wall units. The volume of a big bubble is 1.73 times that of a small bubble. The Eötvös numbers, $Eo = \rho_l g d_0^2/\sigma$, for the small and big bubbles are 0.31 and 0.45, respectively. Ignoring the slight difference in the Morton numbers and assuming that our bubbles are air bubbles in water, then the Eötvös number used here corresponds to bubbles of a diameter of 1.53 and 1.84 mm, respectively. The channel width is eight times the diameter of small bubbles, or 12.24 mm, and the corresponding channel length in the streamwise direction is 19.22 and 9.61 mm in the spanwise direction. The channel Reynolds number of 3786 corresponds to an average velocity of 0.31 m/s. A comparison of the parameters used here with real water-bubbles is shown in Table 1.The bubble response time τ_b can be determined according to Stokes drag law as $\tau_b = d_0^2/36\nu_l$, and we therefore get $\tau_b = 5.21$ for small bubbles and 7.50 for big bubbles. The Kolmogorov time scale of the turbulent flow is given by $\tau_k = (\nu_l/\varepsilon)^{1/2}$, where ε is the turbulent energy dissipation rate, which can be calculated from the flow velocity field or can be determined from $\varepsilon = (u^+)^3/ky_b$, here, $k = 0.42$ is the von Karman constant and y_b is the bubbles' average distance away from the wall. By assuming $y_b = 0.5$, we get $\varepsilon = 3.64 \times 10^{-4}$ and $\tau_k = 0.96$ for the turbulent flow. The Stokes numbers, $St = \tau_b/\tau_k$, are therefore 5.44 and 7.83 for the small and the big bubbles, respectively.

For a bubbly flow, the domain consists of bubbles and liquid which are separated by an immiscible phase boundary with a constant surface tension. The "one fluid" Navier–Stokes equations, valid for the whole domain and incorporating the jump conditions at the interfaces, are

$$\rho\frac{\partial \mathbf{u}}{\partial t} + \rho\nabla\cdot\mathbf{uu} = -\nabla p + (\rho-\rho_0)\mathbf{g} + \nabla\cdot\mu(\nabla\mathbf{u} + \nabla\mathbf{u}^{\mathrm{T}}) + \sigma\int_F \kappa_f \mathbf{n}_f \delta_f(\mathbf{x}-\mathbf{x}_f)\,\mathrm{d}A_f. \quad (2)$$

Here, $\mathbf{u}$ is the velocity vector, p is the pressure, and ρ and μ are the discontinuous density and viscosity fields, respectively, $\mathbf{g}$ is the gravity acceleration, σ is the constant surface tension, and δ_f is a three-dimensional delta function constructed by repeated multiplication of one-dimensional delta functions. κ_f is twice the mean curvature, $\mathbf{n}_f$ is a unit vector normal to the front, $\mathbf{x}$ is the point at which the equation is evaluated, and $\mathbf{x}_f$ is the position of the front. Because of the incompressibility of the liquid and bubbles, the mass conservation equation reduces to

$$\nabla\cdot\mathbf{u} = 0 \quad (3)$$

for the entire domain. When combined with the momentum equation, Eq. (3) leads to a nonseparable elliptic equation of the pressure. We also take the density and viscosity of each fluid to be constants.

These equations are solved by a second-order accurate front-tracking/finite-volume method on a fixed, staggered grid. The original method has been described in detail by Unverdi and Tryggvason (1992) and Tryggvason et al. (2001), and additional validation tests are described by Esmaeeli and Tryggvason (1998, 1999). A comparison between this method and a lattice Boltzman method (LBM) showed that results for the rise of a single bubble are in good agreement (Sankaranarayanan et al., 2003). The current simulations are done using a fully parallel code written in Fortran 90/95 for the simulations described by Bunner and Tryggvason (2002a). Three major changes were, however, necessary for simulations of bubbles in a turbulent channel flow. First, nonuniform grids in the wall-normal direction are used to accommodate the high resolution needed for the turbulent boundary layer. Second, a third-order upwind scheme (QUICK) (Leonard, 1979) is used for the advection terms. It not only increases the accuracy, but also prevents unphysical oscillations in high strain regions of the flow. Third, a nonconservative form of the governing equations is used in the new code. The conservative form used by Bunner and Tryggvason (2002a) is found to cause increasing irregularities in the velocities near the interface for high Reynolds

number flows (Esmaeeli and Tryggvason, 2005). The new code was tested extensively by comparing it with the original code (which has been thoroughly validated) and by grid refinement studies. It has successfully been used in our simulations of bubble-induced drag reduction (Lu et al., 2005).

The simulations were done using grids with $192 \times 160 \times 96$ grid points, uniformly spaced in the x- and z-direction but stretched in the y-direction by a hyperbolic tangent function

$$y(j) = -\frac{\tanh(\gamma(1-2j/N))}{\tanh(\gamma)}, \quad j = 0, 1, \ldots, N. \tag{4}$$

Here, $N = 160$ is the number of grid points in the wall-normal direction and γ is the stretching parameter, which is set to 2.2. The grid spacings in wall units are $\Delta x^+ = \Delta z^+ = 2.08$ for the x- and z-direction, and $0.79 \leqslant \Delta y^+ \leqslant 2.19$ for the y-direction. The initial single phase turbulent flow was the same as that used in Lu et al. (2005). By continuing the simulation of the single phase turbulent flow, we confirmed that our code preserved the statistics of the turbulent flow. We also ran one turbulent bubbly flow case using a finer grid with $320 \times 256 \times 160$ grid points, and found that results were essentially the same as those reported here.

3. Results

We performed three simulations of turbulent bubbly flows with different bubble sizes. The average void fractions for these flows are all the same, or about 3% achieved by adjusting the number of bubbles. The other governing parameters of these flows are the same, as listed in the previous section. Case 1 includes 36 small bubbles ($d_0 = 0.25$), Case 2 is a combination of 22 small bubbles ($d_0 = 0.25$) and 8 big bubbles ($d_0 = 0.3$), and Case 3 has 21 big bubbles ($d_0 = 0.3$). The bubbles are spherical initially and introduced into a single phase turbulent flow at time zero, with a distribution of slightly perturbed regular array. Initially the velocity field inside the bubbles is the same as for the original flow, but it quickly adjusts to the presence of the bubbles. As the flow develops, bubbles near the walls are quickly driven toward the center region of the channel by the lift force and by the wall repulsive force. The pressure gradient forces the flow downward and as the bubbles are driven away from the walls, the mixture density in the middle of the channel decreases. Since the bubbles move slower than the surrounding liquid for the downflow, the liquid velocity in the middle is reduced and becomes nearly uniform. If too many bubbles accumulate in the middle of the channel, the mixture starts to rise due to buoyancy, thus creating a shear that drives the bubbles back toward the walls. This migration of bubbles and the interaction between the bubbles and the ambient liquid gradually change the local properties of the flow. Eventually, however, the turbulent bubbly flow reaches an approximately statistically steady state, where the wall shear stress balances the sum of the imposed pressure gradient and the weight of the bubble/liquid mixture. For the present study, we will only show results after the flow has reached an approximately statistically steady state.

A snapshot of the bubble distribution at one time, after the flow has reached an approximately statistically steady state, is shown in Fig. 2 for all three cases. The darker bubbles are the small ones, and the lighter bubbles are the big ones. Isocontours of the vertical fluid velocity, in a plane through the middle of the domain, are also plotted. The bubble distributions are very similar for all three cases. The bubbles are distributed over the middle part of the channel, and a bubbly free zone exists close to each wall. The bubbles show some tendency to form horizontal clusters, especially the small bubbles, but the distribution of the big bubbles in Case 3 is relatively uniform. All the small bubbles look nearly spherical, while most of the big bubbles are slightly elliptical. The average deformation of all the bubbles will be shown later. The velocity of the fluid changes rapidly near the walls, but is relatively uniform in the center. Since the bubbles are rising relative to the liquid, the velocity contours show the wake of several of the bubbles that are located near the plane where we plot the velocity. Although we show the bubble distribution only at a single instance for each case, we have examined it at several other times and generally find that it is similar to what is shown here. Bunner and Tryggvason (2002 a,b) and Esmaeeli and Tryggvason (2005) have simulated homogeneous buoyant bubbly flows and their results show that nearly spherical bubbles often generate horizontal clusters, like those seen in Fig. 2. Horizontal bubble clusters have also been observed experimentally (Figueroa-Espinoza and Zenit, 2005; Zenit et al., 2001).

In Fig. 3, we plot the horizontal (wall-normal) coordinate of all the bubbles versus time for all three cases over a period of 150 time units after the flows have reached approximately statistically steady states. Solid lines denote the small bubbles, and the dotted lines are for the big bubbles. All the bubbles meander in the center region of the channel, and it is clear from the frequent changes in their paths that the bubbles interact strongly with each other. Those bubbles that move toward the walls bounce back quickly. The regions near the walls remain completely free of bubbles and the thicknesses of the two bubble-free zones are almost the same for all the cases. It is clear that the path of both the small and the big bubbles in Case 2 is similar and the paths in Case 1 and Case 3 look the same. Thus we conclude that the bubble sizes in the cases we studied here have little effect on the distribution of the bubbles.

To quantify the deformation of a bubble, we follow Bunner and Tryggvason (2003) and use the square root of the ratio of the largest and the smallest eigenvalue of the second moment of the inertia tensor

$$\chi = (I_{\max}/I_{\min})^{1/2}, \tag{5}$$

where the second moment of the inertia tensor is computed as

$$I_{ij} = \frac{1}{\mathrm{Vol}_b} \int_{\mathrm{Vol}_b} (x_i - x_{i0})(x_j - x_{j0})\, \mathrm{d}V. \tag{6}$$

Here, Vol_b is the volume of the bubble and x_{i0} and x_{j0} are the coordinates of the bubbles in the i- and j-coordinate directions. For a spherical bubble, $\chi = 1$. For an ellipsoidal bubble, χ is approximately equal to the ratio of the longest to the smallest

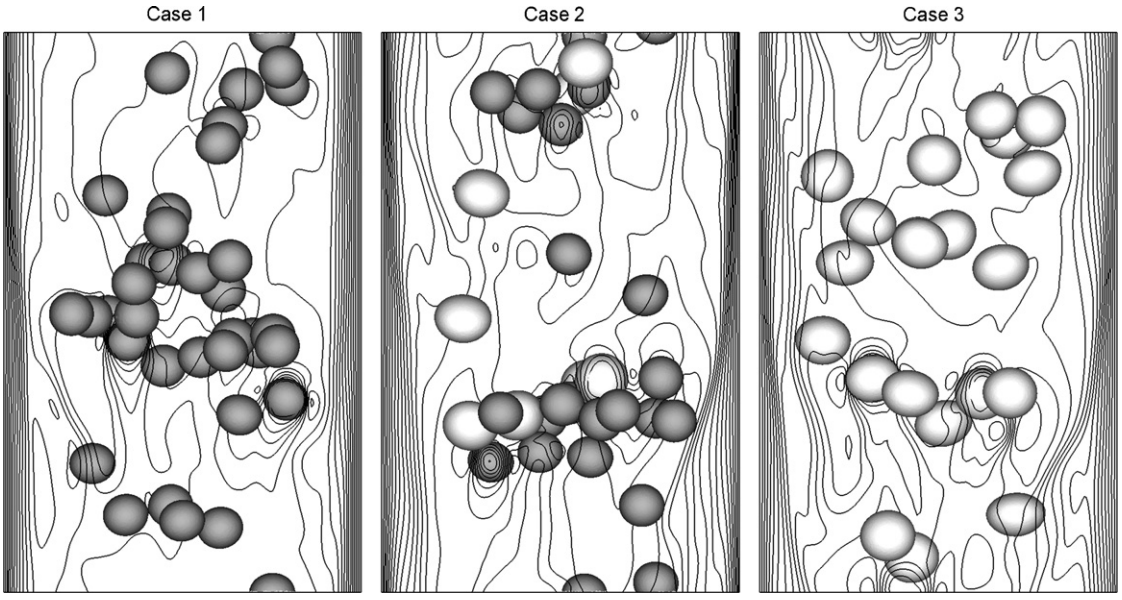

Fig. 2. The bubble distribution and iso-contours of the vertical velocity in the middle plane of the channel. The darker bubbles are the small ones with a diameter of 0.25, and the lighter bubbles are the big ones with a diameter of 0.30.

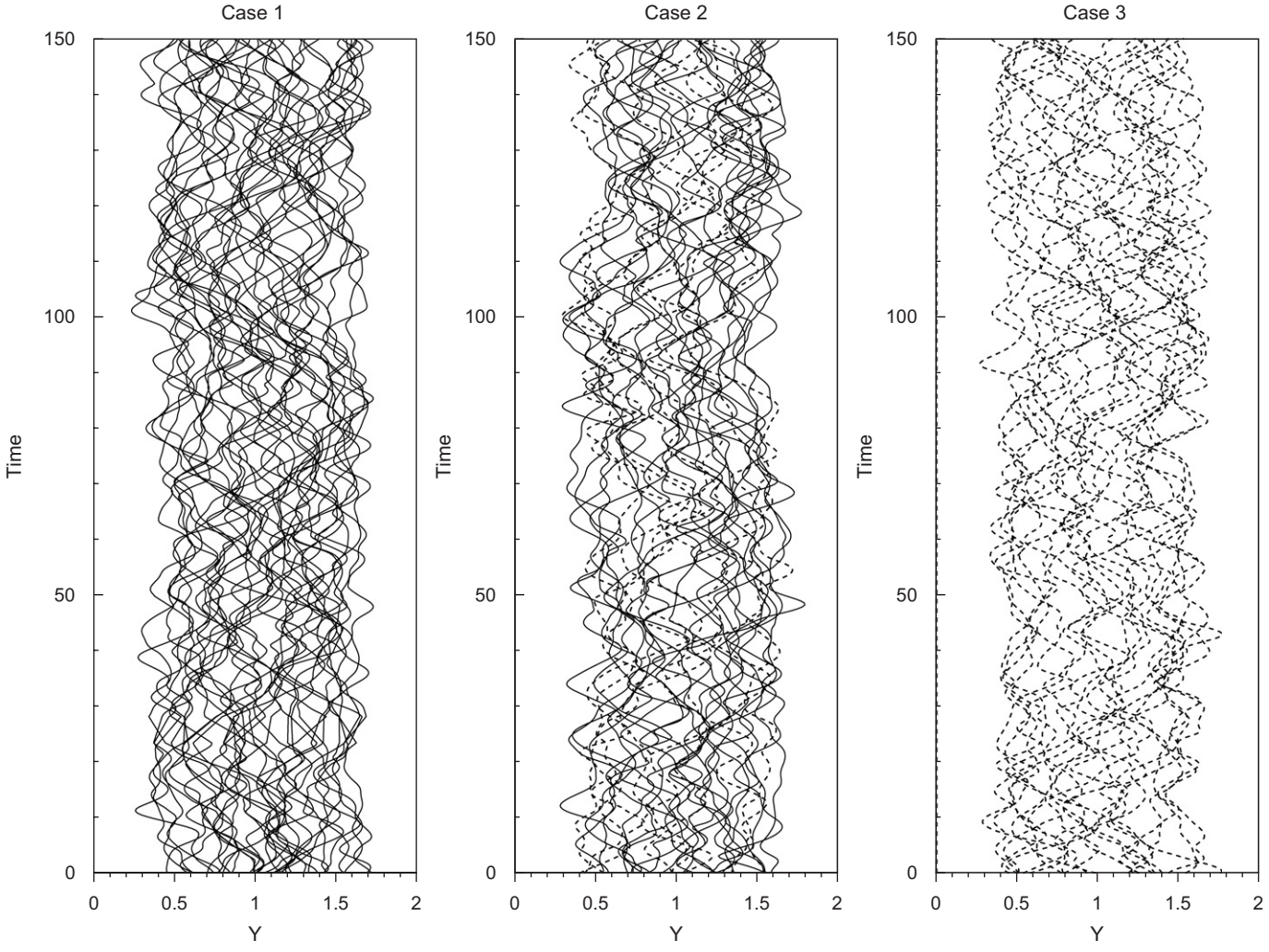

Fig. 3. The path of the bubbles for all three cases. Solid lines denote the small bubbles, and the dotted lines are for the big bubbles.

axis. In Fig. 4, we plot the average deformation of all the bubbles versus the wall-normal coordinate. The circles represent the small bubbles, and the squares denote the big bubbles. The deformations for the small and the big bubbles in Case 2 are also plotted separately. The average deformation is calculated by dividing the width of the channel into 10 equal bins and averaging the bubble deformation in each bin over the same period as in Fig. 3, after the flow has reached a steady state. We have not calculated the deformations for the first two and last two bins, since there are no bubbles in the bins closest to the walls and very few bubbles in the next bins, as seen in Fig. 3. The deformation is almost uniform for the small bubbles, but the values in Case 2 are smaller than those in Case 1. The reason is probably that for Case 2, where both sizes are presented, some small bubbles are located in the wake of the big bubbles. The deformations of the big bubbles in the center are smaller than those in the outer region since they do not encounter any fluid shear there. We note that the deformations of the big bubbles in the bidisperse case are also smaller than those in the monodisperse case.

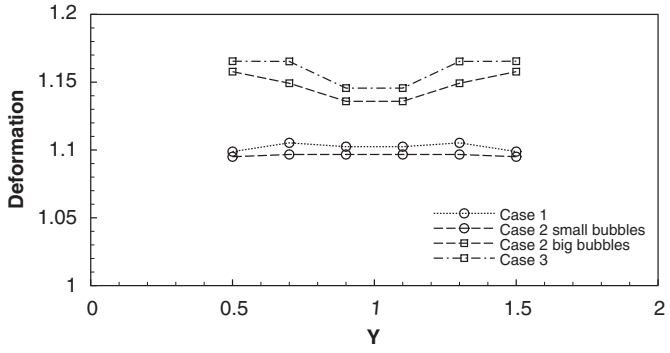

Fig. 4. The average deformation of the bubbles versus the wall-normal coordinate.

We plot the wall shear stress, averaged over both walls, versus time in Fig. 5(a). The time period is the same as in Fig. 3. The averaged wall shear must be balanced exactly by β at statistically steady state. The theoretical value is therefore 0.0036 (2β), and it is clear that the shear stress is close to the theoretical value at all times. The average value also matches it very well. This figure therefore clearly shows that the motion of the bubbly flow has converged very well to a statistically steady state. The mixture flow rate versus time for the same period is plotted in Fig. 5(b). The flow rate is found by averaging the vertical velocity of the mixture over the whole computational domain and then multiplying by the cross-sectional of the domain. The flow rates are essentially constant and almost the same for all the cases. The bubble size therefore has little effect on the flow rate of the mixture, since the average void fractions are almost the same. The flow rates are, however, all lower than the average flow rate for the turbulent flow without bubbles but driven by the same β, which is -1.98.

In our previous study of laminar bubbly flow (Lu et al., 2006), we found that the bubble/liquid mixture in the center region of the channel is in hydrostatic equilibrium. The void fraction distribution of the bubbly channel flow is therefore easily predicted. In hydrostatic equilibrium, the void fraction in the center is given by

$$\varepsilon_c = \varepsilon_{\mathrm{av}} + \frac{\beta}{g\Delta\rho}, \tag{7}$$

and the thickness of the bubble-free zone for the downward flow can be calculated from mass conservation, giving

$$w_{\mathrm{wall}} = \frac{-\beta\delta}{(\beta + \varepsilon_{\mathrm{av}} g\Delta\rho)}. \tag{8}$$

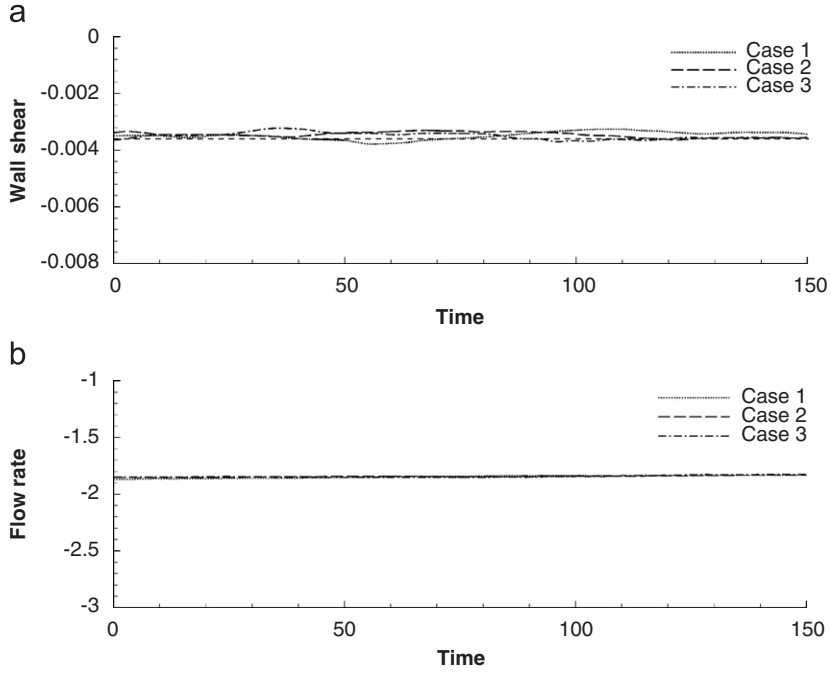

Fig. 5. (a) The average wall shear stress versus time at a statistically steady state. (b) The total mixture flow rate (liquid and bubbles) versus time at a statistically steady state.

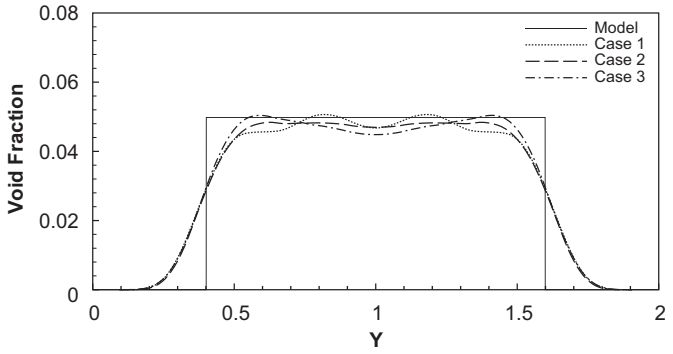

Fig. 6. The average void fraction profile versus the wall-normal coordinate for all three cases. The solid line represents the prediction from the hydrostatic model given by Eq. (7).

Here, ε_{av} is the average void fraction, $\Delta\rho$ is the difference of densities of bubbles and liquid, g is the gravity and δ is the half-width of the channel. This model shows that the void fraction is not depended on the bubble size at all. We used this approach here to predict the void fraction distribution of the turbulent bubbly flows at statistically steady state. The prediction and the average void fraction profiles from the simulations for all three cases are plotted in Fig. 6. The average void fractions are computed by averaging first over planes parallel to the walls and then over 150 time units. Since the domain is small and the simulated time is relatively short, we have also averaged the left and the right hand side, forcing the profile to be symmetric. The dotted line is for Case 1, the dashed line for Case 2, and the dash-dotted line for Case 3. The void fraction in the center region of the channel is relatively constant as found in many experiments (Wang et al., 1987; Kashinsky and Randin, 1999). The profile predicted using the hydrostatic model, Eq. (7), is shown by the solid line. It is clear that the agreement between the averaged void fraction from the simulations and the predicted value from the model is fairly good, and that the bubble size does not affect the average void fraction profile. The transition from zero void fraction near the walls to the constant void fraction in the center is not as sharp as predicted by the model, and the averaged void fraction in the center region of the channel is not exactly flat as predicted. This is, we believe, due to the relatively larger bubble size compared to the computational domain and the relatively small number of bubbles used in our simulations. Our simulation with a higher average void fraction of 6.0% shows a much flatter void fraction profile in the middle of the channel (Lu and Tryggvason, 2006).

In Fig. 7 we plot the vertical liquid velocity (the velocity multiplied by an indicator function set to unity in the liquid and zero in the bubbles), average over time in the same way as the void fraction in Fig. 6 (solid lines). The dotted lines represent the average vertical velocity profile of the corresponding single phase flow. The average bubble velocity, calculated by averaging over bubbles in equal size bins, as for the average deformations, is also shown in the figure. The first and last bins are

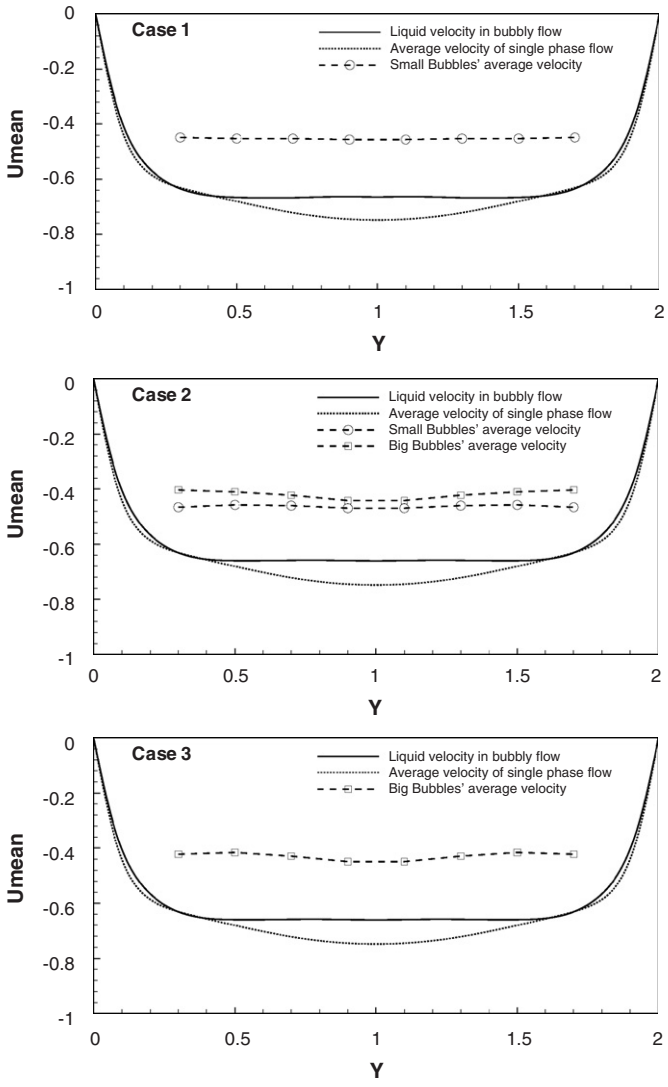

Fig. 7. The average vertical liquid velocity profiles versus the wall-normal coordinate.

empty, since there are no bubbles there for the downward flow. It is clear that the liquid velocity is almost uniform in the middle region of the channel. The average velocity of the bubbles is essentially uniform for the small bubbles, but for the big bubbles the average bubble velocity is smaller at the edge of the center region. This may be due to the slightly larger deformation of the big bubbles there, as can be seen in Fig. 4. The slip velocity of the bubbles is calculated from the difference between the vertical velocity of the bubbles and the corresponding liquid velocity. The average slip velocity of the small bubbles in Case 1 is equal to 0.20. The value for the big bubbles in Case 3 is 0.23 and higher than in Case 1. The average slip velocity for Case 2, with bubbles of two sizes, is 0.20, which is about the same as for Case 1. Considering the big and small bubbles in Case 2 separately, the average slip velocity of the small bubbles is 0.19, slightly lower than in Case 1, and the average slip velocity of the big bubbles is 0.23, the same as for Case 3. Using the formula

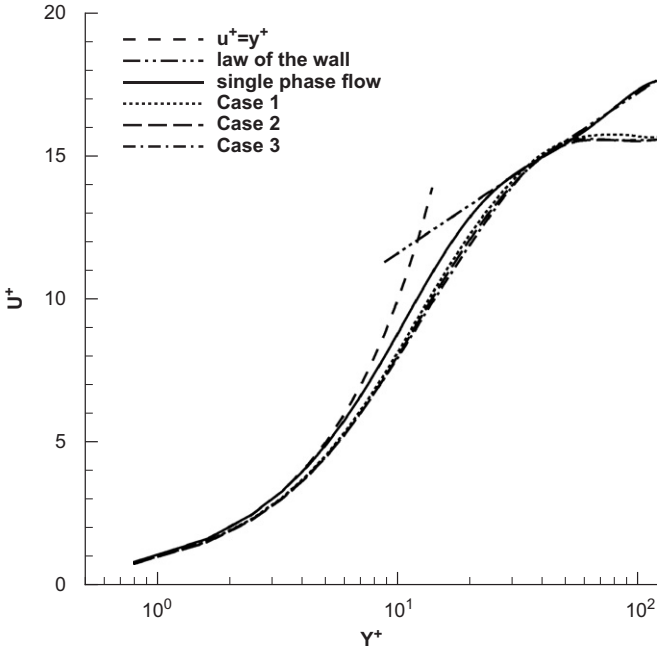

Fig. 8. A semi-log plot of the dimensionless velocity versus the wall-normal coordinate.

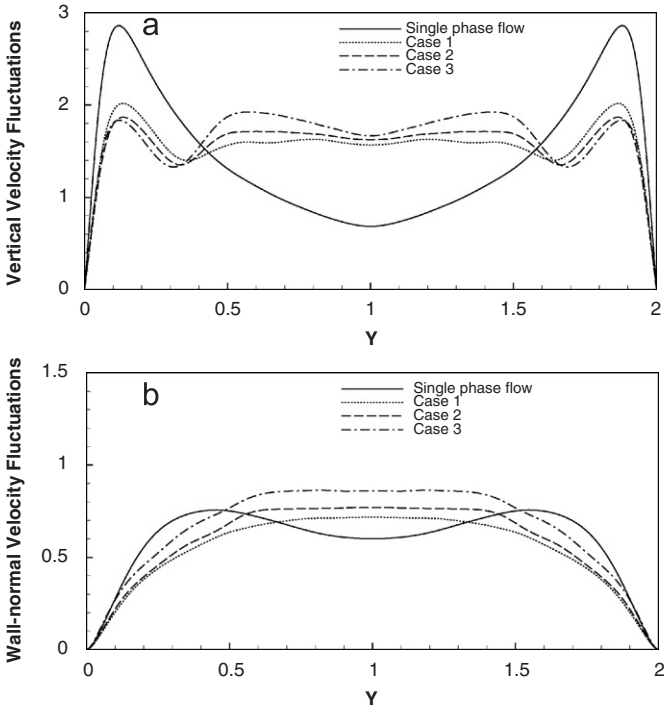

Fig. 9. The root mean square (RMS) velocity fluctuations in the streamwise direction (a) and in the wall-normal direction (b) for all three cases. The velocity fluctuations are normalized by the friction velocity.

suggested by Rodrigue (2001) for the terminal rise velocity of a single bubble in an unbounded fluid and the correlation of Ishii and Zuber (1979) to correct for the effect of a finite void fraction (equal to the average void fraction in the central region of the channel), we obtain slip velocities of 0.18 and 0.20 for the small and big bubbles, respectively. These velocities are smaller than the simulation results, as one would expect since the correlation is based on experimental results for contaminated bubbles.

A semi-log plot of the dimensionless velocities, normalized by the friction velocity u^+, versus the distance from the wall, measured in wall units, is shown in Fig. 8. The logarithmic "law of the wall" $u^+ = (1/\kappa)\ln y^+ + B$, where $\kappa = 0.41$ and $B = 5.95$, is also plotted in the figure. The solid line denotes the mean velocity profile of the corresponding single phase turbulent flow, which agrees very well with the "law of the wall." The profiles for all three cases of bubbly flows are almost identical to each other. In the region of $y^+ \leqslant 54.8$, which is the theoretical thickness of the bubble free-zones in Fig. 6, the velocities of the liquid are slightly lower than for the single phase flow. In the middle of the channel the liquid velocity profiles are flat, unlike the single phase velocity which increases slowly toward the center of the channel. The dimensionless velocities for all cases are almost the same.

The root mean square (RMS) vertical velocity fluctuations for all three cases are plotted in Fig. 9(a) and the corresponding velocity fluctuations in the wall-normal direction are plotted in Fig. 9(b). The averaging approach is the same as for Figs. 5 and 6, and the velocity fluctuations are normalized by the friction velocity. The legends are the same as in Fig. 6. In the bubble-free wall layers, both the vertical and the wall-normal

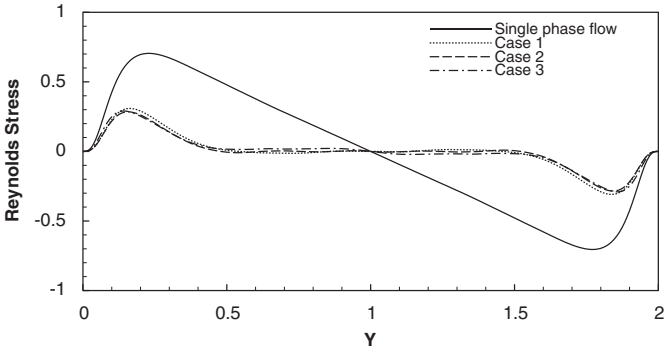

Fig. 10. The average Reynolds stress profile versus the wall-normal coordinate. The Reynolds stress is normalized by the square of the friction velocity.

velocity fluctuations for bubbly flows are lower than the corresponding fluctuations of the single phase flow. The vertical velocity fluctuations in the wall layer do not change with the bubble size, but the wall-normal ones increase with the bubble size. In the middle of the channel, both fluctuations are higher than those of the single phase flow and increase with the bubble size. For Case 2, with the two bubble sizes, the magnitude of the velocity fluctuations is between the corresponding values of the monodispersed small bubbles (Case 1) and big bubbles (Case 3).

In Fig. 10 we plot the average off-diagonal components of the Reynolds stress tensor, $\langle u'v' \rangle$, as a function of the

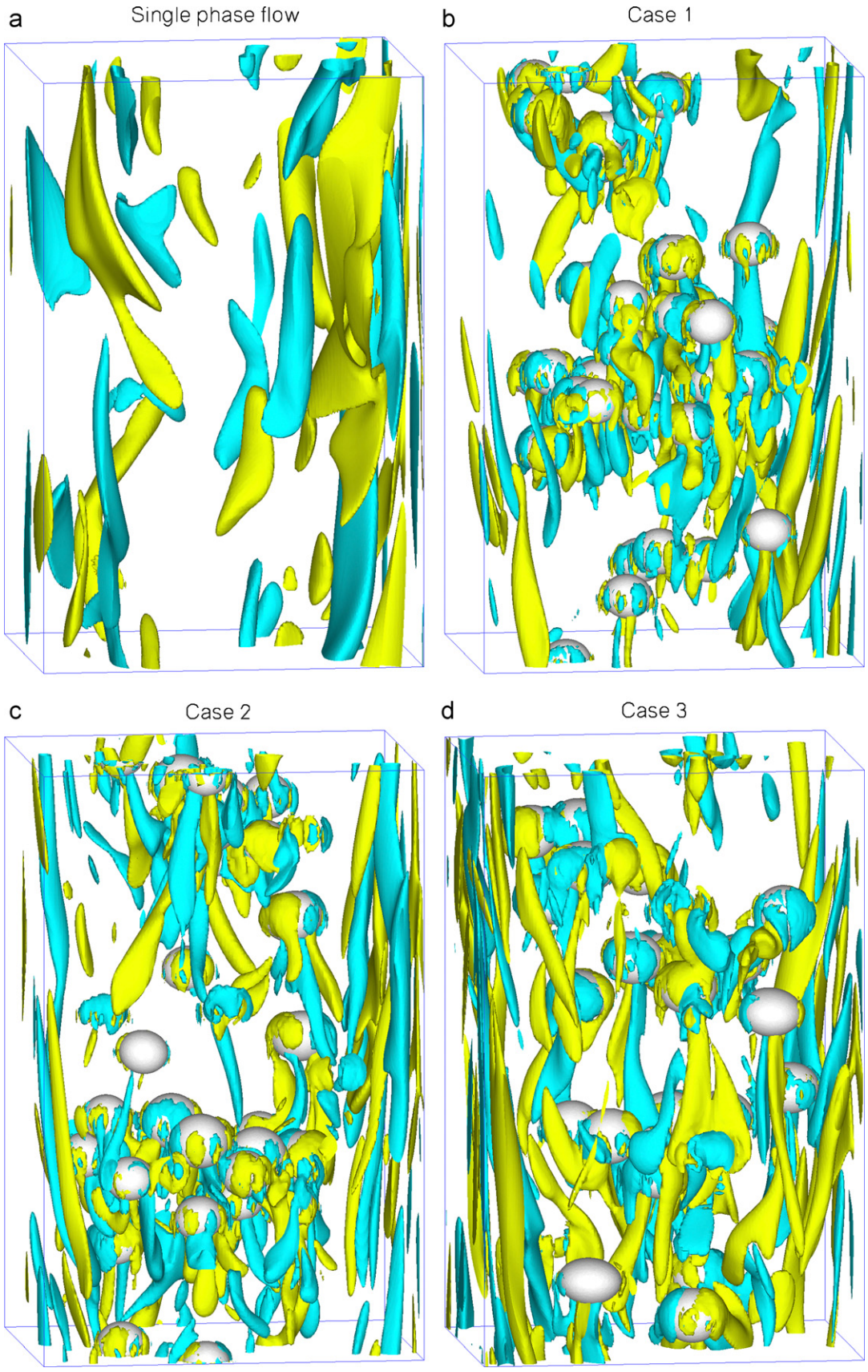

Fig. 11. The bubbles and iso-surfaces of the streamwise vorticity for the single phase flow and three bubbly flows. The yellow iso-surfaces denote the positive streamwise vorticity and the blue green ones are for the negative streamwise vorticity.

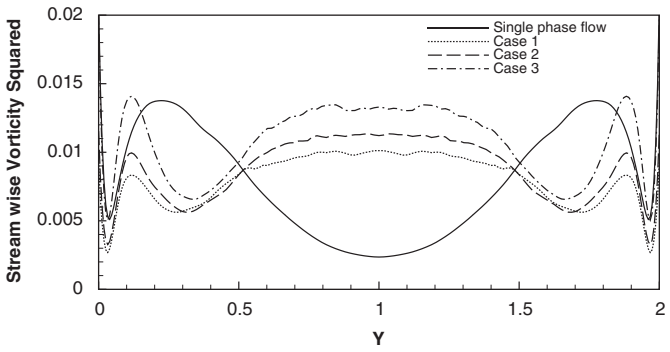

Fig. 12. The streamwise vorticity squared profile versus the cross-channel coordinate. The vorticity is normalized by τ_w/μ.

wall-normal coordinate, normalized by the square of the friction velocity and averaged in the same way as for the velocity and the void fraction plots. We have also averaged over the left and the right hand side of the channel, but taking into account that the fluctuations are antisymmetric around the centerline. For the single phase flow, $\langle u'v' \rangle$ varies linearly across the channel, since the total shear stress must balance the pressure gradient and the viscous contribution to the shear stress is negligible in the core region. For the bubbly flows, on the other hand, $\langle u'v' \rangle$ is almost zero in the middle region of the channel, since the mixture is in hydrostatic equilibrium. Near the walls the flow is bubble-free, but $\langle u'v' \rangle$ is much smaller than for the single phase flow. It is clear that the bubble size has little effect on the Reynolds stress distribution.

In a turbulent channel flow, the wall layer is characterized by the streamwise vortices. The rise of the bubbles also generates a significant amount of vortices. In Fig. 11, the bubbles and isosurfaces of the streamwise vorticity are shown for the single phase flow and the three bubbly flows at one time, as in Fig. 2. The yellow iso-contour surfaces denote positive vorticity and blue green ones indicate negative vorticity. The vortex pairs near the walls for all flows with and without bubbles are clearly visible. However, the vortices are depressed in the bubbly flows compared to the single phase flow. In the middle region of the channel, there are no vortices for the single phase flow, but for the bubbly flows we see significant vorticity although perhaps not as coherent as near the walls. It is clear that the vortices are generated by the bubbles since most of the vortices are located in the wake region of bubbles, and stronger vortices are generated by the big bubbles.

Since the streamwise vorticity is both positive and negative, in Fig. 12 we plot the streamwise vorticity squared (the enstropy), averaged over planes parallel to the walls and over 150 time units, versus the normal-wall coordinate. The enstropy is normalized by $(1/t_0)^2$, where t_0 is a reference time equal to μ/τ_w. The vorticity is very high at the walls for all cases due to the wall-bounded vorticity necessary to bring the velocity induced by the streamwise vorticities to zero. Then there is another maximum in the wall layer due to the streamwise vortices. For the single phase flow, there is then a decline toward the middle of the channel. But for the bubbly flow, the vorticity squared increase again due to the vortices induced by the bubbles. Thus, in the center region of the channel, the vorticity in the bubbly flows is larger than in the single phase flow. But in the wall layer, the vorticity for the case with small bubbles is smaller than in the single phase flow and the vorticity in the case with big bubbles is larger than in the single phase flow. In the whole channel, the big bubbles generate more vorticity than the small bubbles.

4. Conclusions

In this paper we have examined by direct numerical simulations the effect of bubble size on the properties of turbulent bubbly downflow at steady state. We have looked at three systems, one with small bubbles, one with bigger bubbles, and a third with both small and big bubbles. This study complements our earlier study of the effect of void fraction, reported in Lu and Tryggvason (2006). The present results show, as found in the earlier paper, that nearly spherical bubbles migrate away from the walls until the core region of the channel is in hydrostatic equilibrium. The wall layer is free of bubbles and the thickness of the wall layer can be predicted by how much void fraction needs to be added to the core to bring it into hydrostatic equilibrium.

Although the bubble size does have some effects on the turbulent structure of bubbly flows—bigger bubbles generate larger velocity fluctuations in the middle region because the larger slip velocity of the bigger bubbles both perturbs the flow more and results in the deposition of more vorticity into the flow—bubble size has little effect on the void fraction distribution and the liquid mean velocity profile at steady state. The primary role of the bubbles is to reduce the weight of the mixture in the core region and once it is in hydrostatic equilibrium there is no further average migration or lateral transport of the bubbles. Furthermore, the velocity profile is determined by what goes on in the wall layer, where there are no bubbles. In the current simulations, the Stokes numbers $St = \tau_b/\tau_k$ for both bubble sizes examined are larger than 1, so the bubble response time scales are larger than the Kolmogorov time scale. The bubbles therefore do not follow the surrounding liquid and the bubbles are not trapped by the coherent vortices near the walls. Here, all the bubbles move toward the center region of the channel due to the lift force induced by the high shear near the wall. In the center region of the channel, the flow is essentially homogeneous and most of the vorticity is due to the bubble motion. We note that Göz et al. (2001) showed that the difference between homogeneous flows with bubbles of two sizes and flows with only one size were relatively small, as long as the size difference was not too large and the void fraction was the same.

Although the simulations carried out here are limited to only one low void fraction, we have already carried out some preliminary simulations with average void fractions up to 6% and got similar results. The results presented here should be helpful for further development of models for multiphase flow.

Acknowledgments

This study was funded by the Department of Energy, Grant DE-FG02-03ER46083. The simulations reported here are carried out using computer time provided by the National Partnership for Advance Computational Infrastructure, NPACI.

References

Bankoff, S.G., 1960. A variable density single-fluid model for two-phase flow with particular reference to steam-water flow. Journal of Heat Transfer 82, 265–270.

Bunner, B., Tryggvason, G., 2002a. Dynamics of homogeneous bubbly flows. Part 1. Rise velocity and microstructure of the bubbles. Journal of Fluid Mechanics 466, 17–52.

Bunner, B., Tryggvason, G., 2002b. Dynamics of homogeneous bubbly flows. Part 2. Velocity fluctuations. Journal of Fluid Mechanics 466, 53–84.

Bunner, B., Tryggvason, G., 2003. Effect of bubble deformation on the properties of bubbly flows. Journal of Fluid Mechanics 495, 77–118.

Clark, N.N., Flemmer, R.L., 1985. Predicting the holdup in two-phase bubble upflow and downflow using the Zuber and Findlay drift-flux model. A.I.Ch.E. Journal 31, 500–503.

Drew, D.A., Lahey, R.T., 1979. Application of general constitutive principles to the derivation of multidimensional two-phase flow equations. International Journal of Multiphase Flow 5, 243–264.

Drew, D.A., Lahey, R.T., 1982. Phase-distribution mechanisms in turbulent low-quality two-phase flow in a circular pipe. Journal of Fluid Mechanics 117, 91–106.

Esmaeeli, A., Tryggvason, G., 1998. Direct numerical simulations of bubbly flows. Part 1. Low Reynolds number arrays. Journal of Fluid Mechanics 377, 313–345.

Esmaeeli, A., Tryggvason, G., 1999. Direct numerical simulations of bubbly flows. Part 2. Moderate Reynolds number arrays. Journal of Fluid Mechanics 385, 325–358.

Esmaeeli, A., Tryggvason, G., 2005. A direct numerical simulation study of the buoyant rise of bubbles at (O100) Reynolds number. Physics of Fluids 17, 093303.

Felton, K., Loth, E., 2002. Diffusion of spherical bubbles in a turbulent boundary layer. International Journal of Multiphase Flow 28, 69–92.

Figueroa-Espinoza, B., Zenit, R., 2005. Clustering in high Re monodispersed bubbly flows. Physics of Fluids 17, 091701.

Göz, M.F.G., Bunner, B., Sommerfeld, M., Tryggvason, G., 2001. Direct numerical simulation of bidisperse bubble swarms. In: ICMF-2001 Fourth International Conference on Multiphase Flow, May 27–June 1, 2001, New Orleans, LA.

Ishii, M., Zuber, N., 1979. Drag coefficient and relative velocity in bubbly droplet, or particulate flows. A.I.Ch.E. Journal 25, 843–855.

Jimenez, J., Moin, P., 1991. The minimal flow unit in near-wall turbulence. Journal of Fluid Mechanics 225, 213–240.

Kashinsky, O.N., Randin, V.V., 1999. Downward bubbly gas–liquid flow in a vertical pipe. International Journal of Multiphase Flow 25, 109–138.

Leonard, B.P., 1979. A stable and accurate convective modelling procedure based on quadratic upstream interpolation. Computer Methods in Applied Mechanics and Engineering 19, 59–98.

Levy, S., 1963. Prediction of two-phase pressure drop and density distributor from mixing length theory. Journal of Heat Transfer 85, 137–152.

Liu, T.J., 1993. Bubble size and entrance length effects on void development in a vertical channel. International Journal of Multiphase Flow 19, 99–113.

Liu, T.J., 1997. Investigation of the wall shear stress in vertical bubbly flow under different bubble size conditions. International Journal of Multiphase Flow 23, 1085–1109.

Liu, T.J., Bankoff, S.G., 1993a. Structure of air–water bubbly flow in a vertical pipe. Part 1, liquid mean velocity and turbulence measurements. International Journal of Heat and Mass Transfer 36, 1049–1060.

Liu, T.J., Bankoff, S.G., 1993b. Structure of air–water bubbly flow in a vertical pipe. Part 2, void fraction, bubble velocity and bubble size distribution. International Journal of Heat and Mass Transfer 36, 1061–1072.

Lopez de Bertodano, M., Lahey, R.T.J., Jones, O.C., 1994. Phase distribution in bubbly two-phase flow in vertical ducts. International Journal of Multiphase Flow 20, 805–818.

Lu, J., Tryggvason, G., 2006. Numerical study of turbulent bubbly downflows in a vertical channel. Physics of Fluids 18, 103302.

Lu, J., Fernandez, A., Tryggvason, G., 2005. The effect of bubbles on the wall drag in a turbulent channel flow. Physics of Fluids 17, 095102.

Lu, J., Biswas, S., Tryggvason, G., 2006. A DNS study of laminar bubbly flows in a vertical channel. International Journal of Multiphase Flow 32, 643–660.

Nakoryakov, V.E., Kashinsky, O.N., Randin, V.V., Timkin, L.S., 1996. Gas–liquid bubbly flow in vertical pipes. Journal of Fluids Engineering—Transactions of the ASME 118, 377–382.

Oshinowo, T., Charles, M.E., 1974. Vertical two-phase flow. II. Holdup and pressure drop. Canadian Journal of Chemical Engineering 52, 438–448.

Politano, M.S., Carrica, P.M., Converti, J., 2003. A model for turbulent polydisperse two-phase flow in vertical channels. International Journal of Multiphase Flow 29, 1153–1182.

Rodrigue, D., 2001. Generalized correlation for bubble motion. A.I.Ch.E. Journal 47, 39–44.

Sankaranarayanan, K., Kevrekidis, I.G., Sundaresan, S., Lu, J., Tryggvason, G., 2003. A comparative study of lattice Boltzman and front-tracking finite-difference methods for bubble simulations. International Journal of Multiphase Flow 29, 109–116.

Serizawa, A., Kataoka, I., Michiyoshi, I., 1975a. Turbulence structure of air–water bubbly flow. II. Local properties. International Journal of Multiphase Flow 2, 235–246.

Serizawa, A., Kataoka, I., Michiyoshi, I., 1975b. Turbulence structure of air–water bubbly flow. III. Transport properties. International Journal of Multiphase Flow 2, 247–259.

Stewart, C.W., 1995. Bubble interaction in low-viscosity liquids. International Journal of Multiphase Flow 21, 1037–1046.

Sun, X., Paranjape, S., Kim, S., Ozar, B., Ishii, M., 2004. Liquid velocity in upward and downward air–water flows. Annals of Nuclear Energy 31, 357–373.

Tomiyama, A., Tamai, H., Zun, I., Hosokawa, S., 2002. Transverse migration of single bubbles in simple shear flows. Chemical Engineering Science 57, 1849–1858.

Tryggvason, G., Bunner, B., Esmaeeli, A., Juric, D., Al-Rawahi, N., Tauber, W., Han, J., Nas, S., Jan, Y.J., 2001. A front-tracking method for the computations of multiphase flow. Journal of Computational Physics 169, 708–759.

Unverdi, S.O., Tryggvason, G., 1992. A front-tracking method for viscous incompressible multi-fluid flows. Journal of Computational Physics 100, 25–37.

Wang, S.K., Lee, S.J., Jones, O.C.J., Lahey, R.T.J., 1987. 3-D Turbulence structure and phase distribution measurements in bubbly two-phase flows. International Journal of Multiphase Flow 13, 327–343.

Zenit, R., Koch, D.L., Sangani, A.S., 2001. Measurements of the average properties of a suspension of bubbles rising in a vertical channel. Journal of Fluid Mechanics 429, 307–342.